

Universal response of the type-II Weyl semimetals phase diagram

P. Rüßmann,¹ A. P. Weber,^{2,3} F. Glott,⁴ N. Xu,^{2,3} M. Fanciulli,^{2,3} S. Muff,^{2,3} A. Magrez,²
P. Bugnon,² H. Berger,² M. Bode,⁴ J. H. Dil,^{2,3} S. Blügel,¹ P. Mavropoulos,¹ and P. Sessi^{4,*}

¹*Peter Grünberg Institut and Institute for Advanced Simulation,
Forschungszentrum Jülich and JARA, 52425 Jülich, Germany*

²*Institute of Physics, École Polytechnique Fédérale
de Lausanne, 1015 Lausanne, Switzerland*

³*Swiss Light Source, Paul Scherrer Institute, 5232 Villigen-PSI, Switzerland*

⁴*Physikalisches Institut, Experimentelle Physik II,
Universität Würzburg, Am Hubland, D-97074 Würzburg, Germany*

(Dated: June 5, 2017)

Abstract

The discovery of Weyl semimetals represents a significant advance in topological band theory. They paradigmatically enlarged the classification of topological materials to gapless systems while simultaneously providing experimental evidence for the long-sought Weyl fermions. Beyond fundamental relevance, their high mobility, strong magnetoresistance, and the possible existence of even more exotic effects, such as the chiral anomaly, make Weyl semimetals a promising platform to develop radically new technology. Fully exploiting their potential requires going beyond the mere identification of materials and calls for a detailed characterization of their functional response, which is severely complicated by the coexistence of surface- and bulk-derived topologically protected quasiparticles, i.e., Fermi arcs and Weyl points, respectively. Here, we focus on the type-II Weyl semimetal class where we find a stoichiometry-dependent phase transition from a trivial to a non-trivial regime. By exploring the two extreme cases of the phase diagram, we demonstrate the existence of a universal response of both surface and bulk states to perturbations. We show that quasi-particle interference patterns originate from scattering events among surface arcs. Analysis reveals that topologically non-trivial contributions are strongly suppressed by spin texture. We also show that scattering at localized impurities generate defect-induced quasiparticles sitting close to the Weyl point energy. These give rise to strong peaks in the local density of states, which lift the Weyl node significantly altering the pristine low-energy Weyl spectrum. Visualizing the microscopic response to scattering has important consequences for understanding the unusual transport properties of this class of materials. Overall, our observations provide a unifying picture of the Weyl phase diagram.

The discovery of topological insulators (TIs) [1, 2] led to intense research efforts in searching for materials whose properties are determined by band structure topology. In this context, the recent discovery of Weyl semimetals represents a milestone [3, 4]. Contrary to TIs, where topological properties only are only manifested at boundaries as gapless Dirac states, Weyl semimetals host bulk as well as surface topologically protected quasiparticles. In particular, Weyl points appear at crossing points that are protected by the topology of the bulk band structure. Because of the well-known surface-to-bulk correspondence, they are necessarily associated to the appearance of new topologically protected boundary modes at the surface, the so-called topological Fermi arcs, which occupy unclosed Fermi contours connecting Weyl points of opposite chirality [5, 6].

Beyond their fundamental relevance, Weyl semimetals are characterized by intriguing transport properties. Very high mobility, extremely strong magnetoresistance [7], and even more exotic phenomena such as the chiral anomaly [8] or the possibility for Fermi arcs to tunnel through the bulk via the Weyl points have been discussed [9]. Because of the robustness inherited from topological protection, these effects are raising great expectations for direct applications of these materials in spintronics and magneto-electrics.

Weyl semimetals have been first experimentally discovered in the TaAs monpnictide family, known as type-I [3, 4, 10–14]. More recently, it has been suggested that once Lorentz invariance is broken, a new flavor of Weyl material can be realized, the so-called type-II, where strongly tilted Weyl cones emerge at the boundaries between bulk electron and hole pockets [15]. Theoretical predictions identified the $\text{Mo}_x\text{W}_{1-x}\text{Te}_2$ family as promising compounds [15–18]. One of the most interesting aspects of type-II Weyl materials is the possibility to continuously tune their topological properties by acting onto their stoichiometry [18]. The resulting phase diagram offers an ideal platform to explore the functional response of the electronic properties and the existence of unifying trends within the Weyl phase.

The $\text{Mo}_x\text{W}_{1-x}\text{Te}_2$ family is characterized by a layered structure which crystallizes in a T_d orthorhombic cell lacking inversion symmetry at low temperatures (space group $Pmn2_1$) [19]. The transition metal (W and Mo) planes are separated by Te bilayers as shown in Fig. 1(a). Adjacent Te–(W/Mo)–Te trilayers are weakly bound by van der Waals forces thus offering a natural cleaving plane. As a result, the surface exposed after cleaving is always Te-terminated. As illustrated in Fig. 1(a), the Te atoms occupy two inequivalent

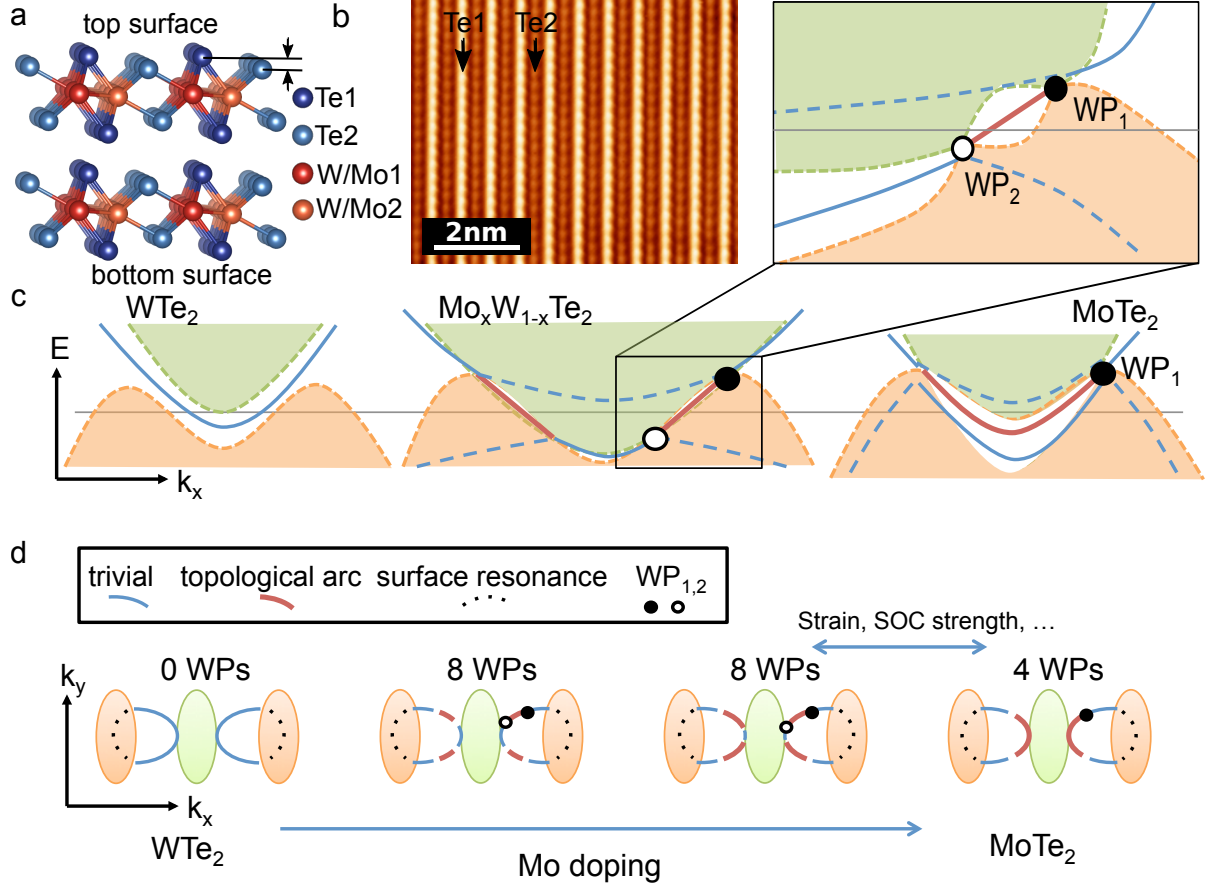


FIG. 1: **a** Crystal structure of MoTe₂ and WTe₂; **b** Atomically resolved STM topography of the WTe₂ surface. The existence of two inequivalent Te sites labelled Te1 and Te2 with Te1 being slightly higher than Te2 gives rise to the column-like character visible in the STM image. **c** Schematic representation of the type-II Weyl phase diagram. Although being topologically trivial, WTe₂ is found to lie very close to the topological phase transition. Consequently, small lattice distortions can easily drive WTe₂ into a Weyl phase. By starting from WTe₂ and substituting W with Mo, the system enters into a progressively more stable Weyl phase. **d** Evolution of the topological Fermi arcs as a function of the Mo concentration. By increasing the Mo concentration, topological Fermi arcs (red lines) become progressively larger.

sites, labelled Te1 and Te2, with one slightly protruding over the other. This is reflected in the column-like character visible in the atomically resolved STM image reported in Fig. 1(b).

Density functional theory calculations indicated how, by starting from WTe₂—which lies close to a topological phase transition—and substituting W with Mo, the system enters into a progressively more stable Weyl phase as schematically illustrated in Fig. 1(c) [18]. In

particular, by increasing the Mo concentration, the Weyl points become well-separated in reciprocal space and thus cannot easily be annihilated by small perturbations [18]. The larger Weyl point separation has direct consequences for the surface, with topological Fermi arcs getting progressively larger [see red lines in Fig. 1(d)]. In this respect, it is worth noticing that the surface electronic structure of these compounds is substantially complicated by the concomitant existence of trivial surface states. Although they do not form open arcs, trivial states partially overlap with the projected bulk electronic structure, giving rise to surface resonances [dashed lines in Fig. 1(d)] which are characterized by a reduced surface spectral weight. As a result, their pure surface state part (blue line) can effectively mimic an open arc-like contour.

Experimentally investigating this phase diagram proved problematic. This is mainly due to two reasons: (i) Contrary to type-I Weyl materials, in type-II, the projection of the Weyl points onto the surface is overlapping with several bulk-derived trivial states, thereby complicating the discrimination of topological Fermi arcs from other states of trivial origin [20–27]; (ii) The Weyl points are expected to appear at energies above the Fermi level [15–18], where they are inaccessible to conventional photoemission techniques [20–27]. In this context, while a general consensus exists over the topological nature of the MoTe_2 arcs [20–22], the situation appears highly controversial for WTe_2 . Although surface arcs have clearly been observed in several photoemission studies, their topological or trivial nature is highly debated with different studies reaching conflicting conclusions [23–26]. *Ab initio* calculations also show that—while MoTe_2 is well inside the Weyl regime [28]— WTe_2 is in close proximity to a Weyl phase transition [23]. This can give rise to Weyl points of opposite chirality which are very close in reciprocal space and thus can easily be annihilated by very small lattice distortions induced by strain or temperature as discussed in Ref. 23. Therefore, it is particularly important to investigate the existence of universal signatures spanning the entire Weyl phase diagram, e.g. by comparing the two extreme cases, MoTe_2 and WTe_2 .

Here, we visualize the response of MoTe_2 and WTe_2 and discuss the results in terms of Weyl nodes and Fermi arcs. We identify the existence of a universal response of these systems to perturbations, which is found to be composition-independent. In particular, we report the emergence of well-defined quasiparticle interference patterns originating from surface arcs. Contrary to earlier studies [22]: (i) we can clearly resolve their open contour and (ii) demonstrate that topological Fermi arc contributions are strongly suppressed because of their

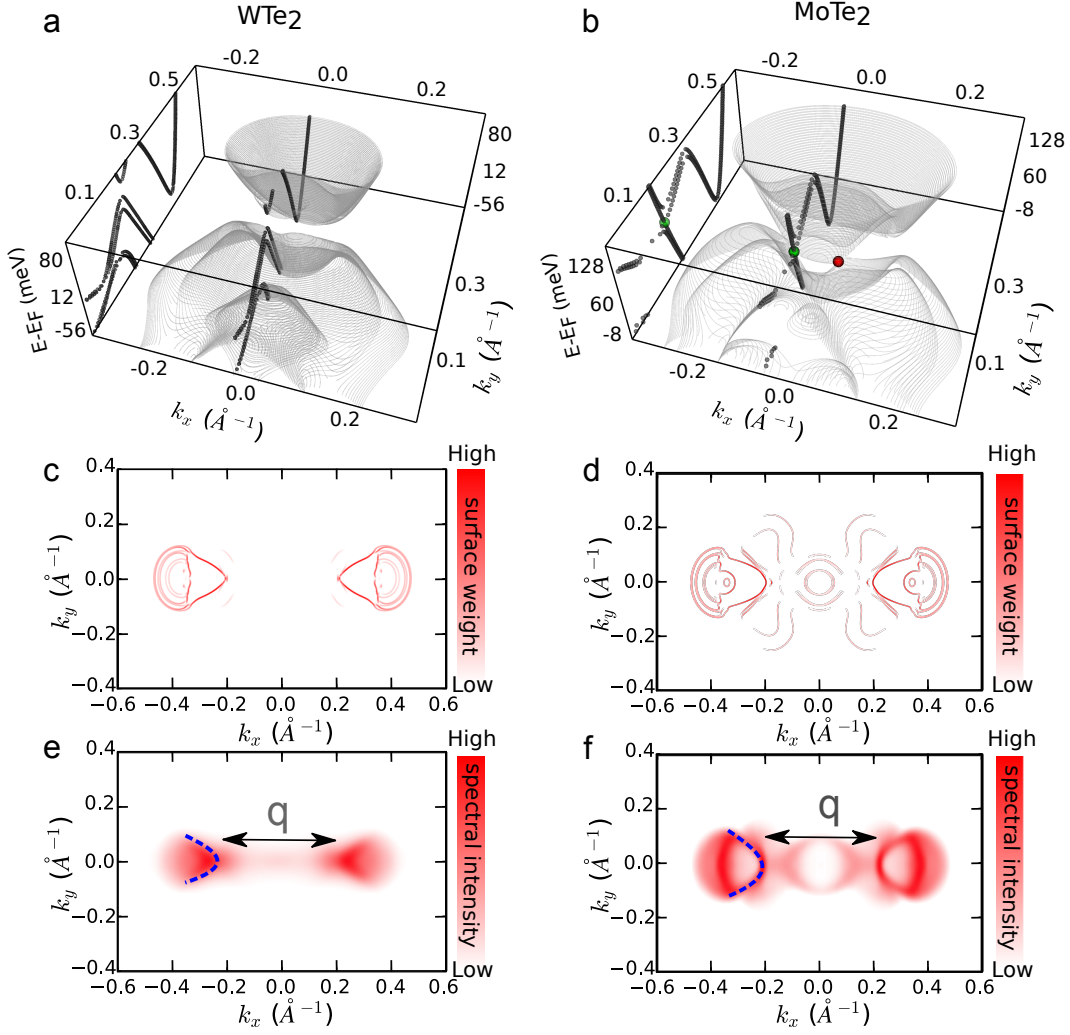


FIG. 2: **a,b** Calculated bulk band structure at $k_z = 0$, **c,d** theoretical and **e,f** experimental Fermi surface for WTe₂ and MoTe₂, respectively. In (a), the dotted lines show the band structure along k_y at the particular k_x where the electron and hole pockets approach each other closest. In (b), the dotted lines show the band structure along k_y at the specific k_x where Weyl points appear (green and red circles, reflection-symmetric around $k_x = 0$). The experimental Fermi surfaces have been obtained by angle-resolved photoemission spectroscopy at a temperature $T < 60$ K using photon energies of 20 and 24 eV for MoTe₂ and WTe₂, respectively.

spin texture which protects them from back-scattering [22, 29]. Furthermore, in line with the theoretical predictions of the response of Weyl semimetals, we reveal the emergence of new quasiparticles arising at the Weyl point energy, which lift the density of states minimum associated to the Weyl node [30, 31].

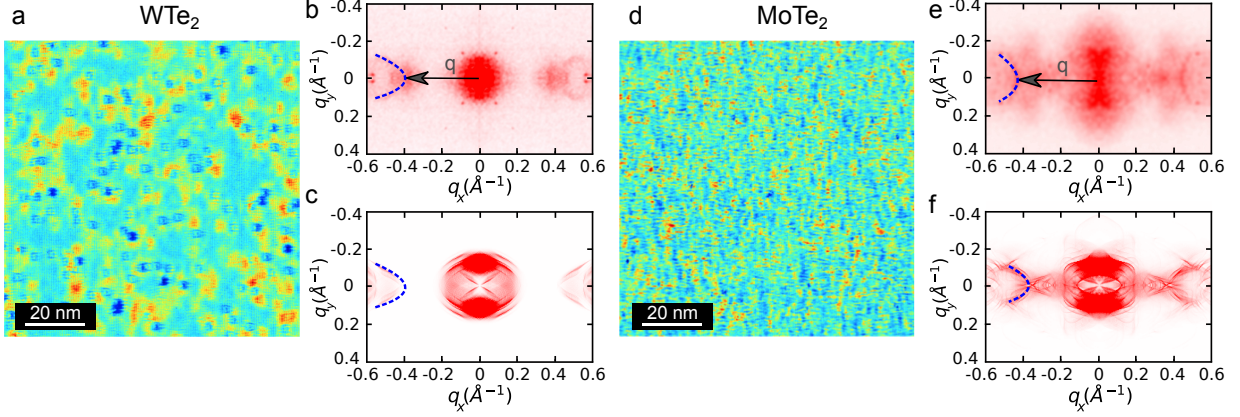


FIG. 3: **a** Differential conductance dI/dU map close to the Fermi ($E - E_F = 10$ meV); **b** Fourier-transformed dI/dU map and **c** theoretically calculated quasi-particle interference pattern obtained on WTe_2 . **d** Differential conductance dI/dU map close to the Fermi ($E - E_F = 10$ meV); **e** Fourier-transformed dI/dU map and **f** theoretically calculated quasi-particle interference pattern obtained on MoTe_2 . The quasi-particle interference pattern is dominated by scattering events between opposite Fermi arcs.

Fig. 2(a,b) report the electronic band structure of bulk WTe_2 and MoTe_2 at $k_z = 0$, respectively, where due to the crystal symmetry Weyl points are possible [15], calculated with the density-functional-based full-potential relativistic Korringa-Kohn-Rostoker Green-function method [32–35], respectively. Computational details can be found in supplementary material. The combined effects of the inversion asymmetry of the crystal structure and the strong spin-orbit coupling characterizing these materials give rise to a spin-polarized band structure [36]. However, whereas Weyl points are emerging in MoTe_2 [see green and red dots in Fig. 2(b) which identify one pair of Weyl points of opposite chirality], a gap between electron and hole pockets is clearly visible for WTe_2 [Fig. 2(a)], indicating the trivial character of this compound. In this context, it is worth noticing that the electronic structure of WTe_2 is very delicate. As discussed in Ref. 18, small changes of the lattice constant can drive the system into a non-trivial state hosting 8 Weyl points, proving the close vicinity of a topological phase transition. Despite these differences highlighted by band structure calculations, our angle-resolved photoemission data reported in Fig. 2(e,f) reveal the presence of arc-like electronic structures in both compounds (see dashed lines). An overall agreement between theory and experiments is found. Although it is tempting

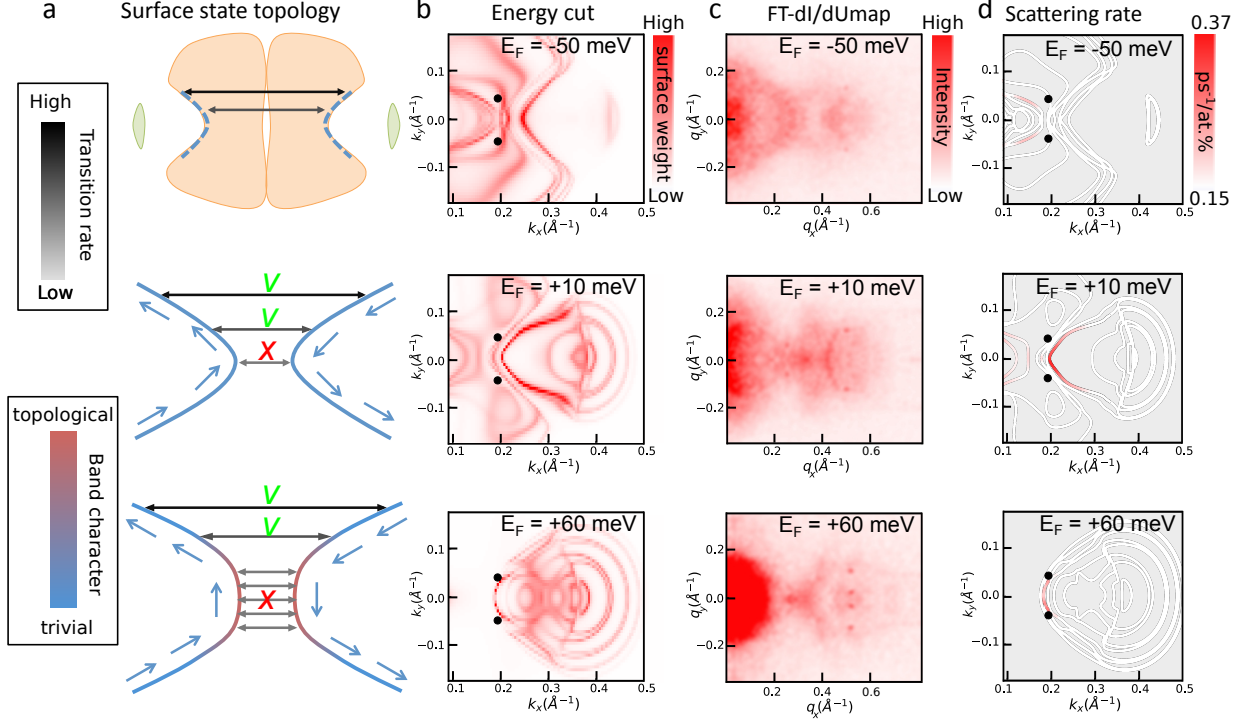


FIG. 4: **a** Schematic representation of the scattering events among Fermi arcs in MoTe₂, **b** theoretically calculated surface-projected constant energy cuts, **c** experimentally obtained Fourier transformed quasi particle interference patterns and **d** theoretically calculated scattering rate. In (b-d) the black dots identify the Weyl points. All results are given for three representative energies: below the Fermi (top panels), close to the Fermi (middle panels), close to the position of the Weyl points, where the extension of the topologically non-trivial arcs is maximized (bottom panels).

to assign the arc-like features in Fig. 2(e,f) to topological Fermi arc states, comparison with calculated constant-energy contours reported in Fig. 2(c,d) reveal a more complicated scenario. Indeed, *ab initio* calculations reveal that several electronic features coexist within a very small part of the first Brillouin zone which cannot fully be resolved by photoemission experiments [37]. It is worth stressing that, as discussed above, an analysis of our calculations reveals that most of the arcs visible in Fig. 2(c,d) are of trivial origin and that only for MoTe₂ also topological Fermi arcs are present. This proves that the observation of surface arcs is a necessary, but not a sufficient condition to unequivocally imply the existence of Weyl points.

To disentangle trivial from topological Fermi arcs contributions, we performed quasi-particle interference experiments. This technique makes use of the standing-wave pattern generated by elastic scattering of electronic states at surface defects and has been proven to

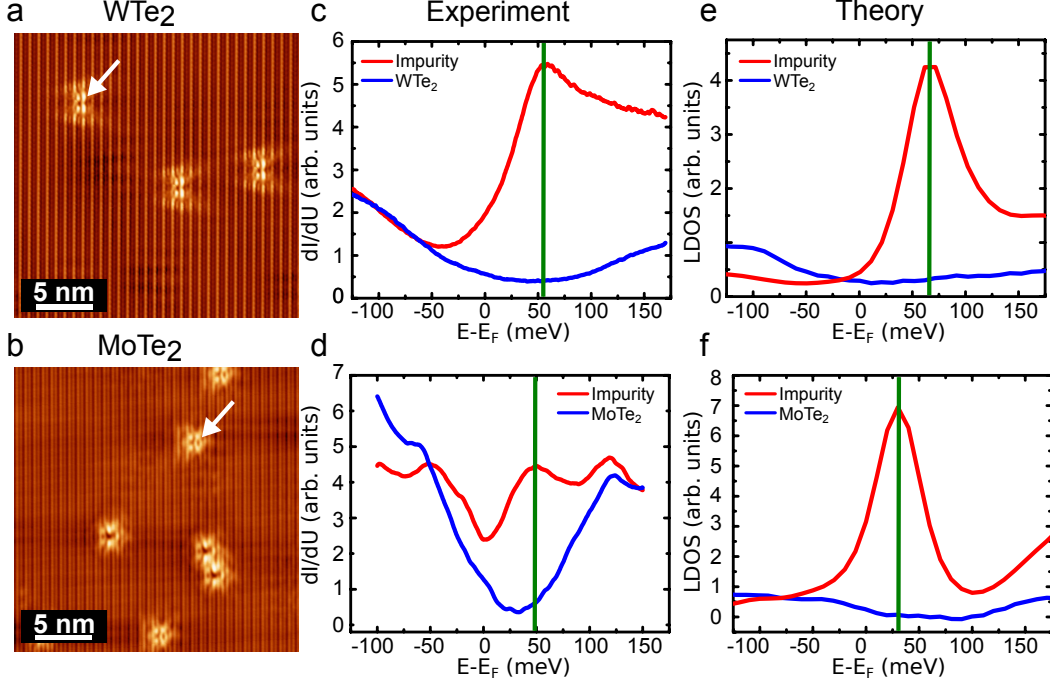


FIG. 5: **a,b** Topographic images acquired on WTe₂ and MoTe₂. In both cases, intrinsic defects are present on the surface. **c,d** Comparison of scanning tunneling spectroscopy data taken on a defect-free area (blue line) and by positioning the tip on top of antisites defects (W and Mo substituting Te) revealing the emergence of quasiparticle resonances close the Weyl point energy (see discussion in the text). **e,f** *Ab-initio* calculated local density of states on the pristine surface (blue line) and on top of an antisite defect (red line) confirm the experimental findings. Green vertical lines are used as marker to identify the position of the peak maximum.

be a powerful method to test the properties of topological materials [38–43]. Contrary to conventional photoemission spectroscopy, it gives access to both occupied and unoccupied electronic states thereby providing a complete spectroscopic characterization of all relevant electronic features around the Fermi energy. This is particularly important for type-II Weyl materials, where Weyl points are theoretically expected to emerge above the Fermi level [15–18]. Fig. 3(a) and (d) report differential conductance dI/dU maps acquired in close proximity of the Fermi level ($E - E_F = 10$ meV) on WTe₂ and MoTe₂, respectively. Their Fourier transformations—reported in panels (b) and (e)—allow to conveniently analyze scattering channels in reciprocal space. Our results reveal the emergence of clear arc-like interference patterns as indicated by the black arrows in both compounds which develop along the q_x direction at approximately $q_x = 0.4 \text{ \AA}^{-1}$ (see dashed blue lines). To shed light on the origin

of these vectors, experimental data have been compared with calculated interference patterns. Our theoretical approach employs the extended-JDOS model [44], with the impurity's electronic structure and scattering amplitude calculated by means KKR method. Results for WTe₂ and MoTe₂ are reported in Fig. 3(c) and (f). As for the experimental results, an arc-like feature is clearly visible in both cases along the q_x direction (see dashed lines), which originates from intra-arc scattering among opposite Fermi arcs. This assignment is further supported by direct comparison with photoemission data [cf. Fig. 2(e,f), where the scattering vector q corresponds to the distance connecting opposite arcs]. Indeed, momentum conservation requires $k_f = k_i + q$, where k_i and k_f are the wave vectors of initial and final states and q is the scattering vector connecting them. A quantitative comparison with the experimental constant energy contours reported in Fig. 2(e,f) allows to directly link these interference phenomena to intra-arc scattering among opposite Fermi arcs. Furthermore, contrary to photoemission data, the higher surface sensitivity of STM unequivocally proves the open contour character of the arcs.

In this context, it is worth noticing that the close proximity of WTe₂ to a Weyl transition allows one to safely exclude any significant contribution of topological Fermi arcs to the observed interference patterns for this compound. Even when considering a slightly distorted structure hosting Weyl points, they would be so close in reciprocal space that the extension of topological Fermi arcs connecting them would be negligible. This is not the case in MoTe₂ where—by progressively moving towards the energy position of the Weyl points—topologically non-trivial Fermi arcs span a much larger fraction of the Brillouin zone. This is illustrated by the schematic representation reported in Fig. 4(a) and the theoretically calculated constant energy cuts displayed in Fig. 4(b). As shown in panel (a), by progressively increasing the energy (from top to bottom panel) the trivial part (blue line) of the arc is absorbed into the bulk electronic band structure whereas the topologically non-trivial arc (red line) dominates the scene. This transition from trivial to topology-dominated Fermi arcs is experimentally investigated in Fig. 4(c). At energies well below the Weyl points (upper panel) only trivial arcs exist. As a consequence, the experimental data show only weak interference patterns. This can be traced back to the combined effect of (i) the V-shape visible in the calculated constant energy contour which results in poor nesting conditions and (ii) the overlap with projected bulk pockets making these states surface resonances that are much less localized at the surface than “real” surface states [cf. top panel of Fig. 4(a)].

By going up in energy, the surface states become well separated from bulk states [cf. middle panel of Fig. 4(a)] while simultaneously getting progressively larger, and thus occupying a larger fraction of the Brillouin zone. As a result, a well-defined arc-like interference pattern appears (see middle panel) which—according to calculations—is dominated by trivial states. By moving to even higher energies we move closer to the Weyl points and the topological Fermi arcs prevail [cf. bottom panel of Fig. 4(a)]. This process is associated to a significant flattening of the arc, where several equivalent vectors can connect opposite parallel segments of the Fermi arcs [see grey arrows in Fig. 4(a), lower panel]. Despite this scenario supporting optimal nesting conditions, the scattering intensity drops (see bottom panel). Comparison with *ab initio* calculations reveals that this effect is directly linked to the spin texture of the topological Fermi arcs. Indeed, as schematically illustrated by the blue arrows in Fig. 4(a), at $E - E_F = +60$ meV the spin polarization is basically pointing in opposite directions for opposite topological Fermi arcs segments (spin-resolved constant-energy contours are reported in the supplementary material). This spin texture results in an effective protection against scattering. Such a behavior is reminiscent of the forbidden backscattering originally discussed in Rashba systems [45] and, more recently, in topological insulators [39]. In the present case, however, the presence of large parallel segments with opposite spin polarization significantly extend the protection well beyond time-reversal symmetry partner states.

These conclusions, which are based on a combined analysis of the spin-resolved band structure and quasi-particle interference mapping, are further quantitatively supported by the calculated scattering rates reported in Fig. 4(d). By progressively increasing the energy, the surface arcs occupy a larger fraction of the Brillouin zone. Consequently, more scattering vectors connecting opposite arcs become possible and the scattering intensity rises (see red line in the middle panel). However, once the topological Fermi arcs set in (lower panel) the scattering intensity drops because of the discussed spin-texture protection mechanism.

Finally, we discuss the effect impurities have on Weyl nodes. Recent theoretical predictions showed that a common characteristic of Dirac-like materials is the emergence of impurity-induced quasiparticles which lift the Dirac node [31]. This behavior has been recently confirmed in topological insulators, where impurity resonances induced by magnetic dopants have been shown to effectively fill the gap which is expected to open at the Dirac point in magnetically ordered samples [46]. A similar behavior has been proposed to arise in Weyl semimetals. In particular, scattering at localized impurities is expected to lift the

Weyl node by inducing new quasiparticle resonances close to the Weyl point energy [30, 31]. The emergence of these quasiparticles has been theoretically proposed as a signature of a Weyl phase. This has been experimentally investigated in Fig. 5, where panels (a) and (b) report topographic images acquired on the two different compounds, i.e., WTe_2 and MoTe_2 . Intrinsic defects highlighted by arrows are visible in both cases. They have been identified as anti-sites (W or Mo atoms substitute Te in the topmost layer) and are commonly found in transition metal dichalcogenides [47–49]. Fig. 5(c,d) reports STS data acquired on both materials by positioning the tip on top (red line) and far away from a defect (blue line). The minimum, visible in proximity to the Fermi level on defect-free areas, highlights the semimetallic character of these compounds. However, on top of defects a strong peak is visible in both materials which lifts the local density-of-states minimum.

These defect-induced quasiparticle resonances appear very close to the energy where Weyl points are expected to emerge (see vertical green line which highlights the peak maximum). These findings are supported by the *ab initio*-calculated local-density-of-states at the impurity atom reported in Fig. 5(e) and (f) for WTe_2 and MoTe_2 , respectively. Both reveal the emergence of quasiparticle resonances located at energies which are in excellent agreement with the experiments. In particular, in MoTe_2 the experimentally observed impurity-induced quasiparticle resonance is positioned at the calculated Weyl point energy ($E - E_F = +48$ meV). As discussed above, for WTe_2 our calculations predict a trivial material near to a topological phase transition into a Weyl phase. In this case, the impurity-induced resonances emerge close to the very narrow energy gap between electron and hole pockets, at an energy where Weyl points are expected to emerge according to Refs. 15, 23, 26. This observation provides strong evidence that topological Weyl transitions are continuous smooth transitions of the global bulk band structure. It follows that, although topological indexes change when driving the system through a topological quantum phase transition, the band structure-dependent experimental observables—such as the impurity-induced resonances reported here—can be continuously tuned, and are not characterized by any discontinuity, i.e., on/off behavior. In this sense, Weyl phase transitions appear to behave similarly to topological insulators phase transitions where, by approaching the critical point at which the bulk band structure becomes inverted, spin-polarized helical surface states progressively emerge within the bulk gap [50].

We would like to stress that the relevance of our observations goes well beyond topological

band-structure aspects. It is long known that disorder, and especially resonant impurities, can significantly impact onto transport properties. Even recently, the presence of defects has been invoked to be at the origin of both positive as well as negative magnetoresistance effects in topological semimetals [51, 52]. In this context, our observations contribute by providing a detailed microscopic picture of the resonant scattering off impurities in type-II Weyl semimetals. In particular, we demonstrate that intrinsic defects significantly alter the local density of states close to the Weyl points, ultimately changing the low-energy spectrum of Weyl semimetals. We conclude that the presence of defects cannot be overstressed and suggest that they play an important role in determining the fascinating transport properties of this class of materials [53, 54].

Overall, we reveal the existence of a universal response of the type-II Weyl semimetals phase diagram. We show that surface arcs dominate the interference pattern, with the topological Fermi arc contribution being strongly suppressed by its spin texture. In agreement with theoretical predictions, we also demonstrated that impurity-induced quasiparticle resonances emerge close to the energy where Weyl points are expected. Our observations highlight that the functional response of both surface and bulk states to perturbations in this class of materials does not depend on whether we have passed the Weyl phase transition or we are simply close to it. This allows to infer the existence of a stoichiometry-independent response to perturbations for type-II Weyl, providing a unifying picture of the type-II Weyl phase diagram.

This work was supported by the Deutsche Forschungsgemeinschaft within SPP 1666 (Grant No. BO1468/21-1 and MA4637/3-1) and through SFB 1170 “ToCoTronics” (project A02). P.R., P.M., and S.B. acknowledge financial support from the VITI project of the Helmholtz Association as well as computational support from the JARA-HPC Supercomputing Centre at RWTH Aachen University.

* corresponding author: sessi@physik.uni-wuerzburg.de

- [1] M. Z. Hasan and C. L. Kane. Colloquium. *Rev. Mod. Phys.*, 82:3045–3067, 2010.
- [2] Xiao-Liang Qi and Shou-Cheng Zhang. Topological insulators and superconductors. *Rev. Mod. Phys.*, 83:1057–1110, 2011.

- [3] Su-Yang Xu, Ilya Belopolski, Nasser Alidoust, Madhab Neupane, Guang Bian, Chenglong Zhang, Raman Sankar, Guoqing Chang, Zhujun Yuan, Chi-Cheng Lee, Shin-Ming Huang, Hao Zheng, Jie Ma, Daniel S. Sanchez, BaoKai Wang, Arun Bansil, Fangcheng Chou, Pavel P. Shibayev, Hsin Lin, Shuang Jia, and M. Zahid Hasan. Discovery of a weyl fermion semimetal and topological fermi arcs. *Science*, 349:613–617, 2015.
- [4] B. Q. Lv, H. M. Weng, B. B. Fu, X. P. Wang, H. Miao, J. Ma, P. Richard, X. C. Huang, L. X. Zhao, G. F. Chen, Z. Fang, X. Dai, T. Qian, and H. Ding. Experimental discovery of weyl semimetal taas. *Phys. Rev. X*, 5:031013, 2015.
- [5] Hongming Weng, Chen Fang, Zhong Fang, B. Andrei Bernevig, and Xi Dai. Weyl semimetal phase in noncentrosymmetric transition-metal monophosphides. *Phys. Rev. X*, 5:011029, 2015.
- [6] Shin-Ming Huang, Su-Yang Xu, Ilya Belopolski, Chi-Cheng Lee, Guoqing Chang, BaoKai Wang, Nasser Alidoust, Guang Bian, Madhab Neupane, Chenglong Zhang, Shuang Jia, Arun Bansil, Hsin Lin, and M. Zahid Hasan. A weyl fermion semimetal with surface fermi arcs in the transition metal monpnictide taas class. *Nature Communications*, 6:7373, 2015.
- [7] Chandra Shekhar, Ajaya K. Nayak, Yan Sun, Marcus Schmidt, Michael Nicklas, Inge Leermakers, Uli Zeitler, Yurii Skourski, Jochen Wosnitza, Zhongkai Liu, Yulin Chen, Walter Schnelle, Horst Borrmann, Yuri Grin, Claudia Felser, and Binghai Yan. Extremely large magnetoresistance and ultrahigh mobility in the topological weyl semimetal candidate nbp. *Nat. Phys.*, 11:645–649, 2015.
- [8] Xiaochun Huang, Lingxiao Zhao, Yujia Long, Peipei Wang, Dong Chen, Zhanhai Yang, Hui Liang, Mianqi Xue, Hongming Weng, Zhong Fang, Xi Dai, and Genfu Chen. Observation of the chiral-anomaly-induced negative magnetoresistance in 3d weyl semimetal taas. *Phys. Rev. X*, 5:031023, 2015.
- [9] Andrew C. Potter, Itamar Kimchi, and Ashvin Vishwanath. Quantum oscillations from surface fermi arcs in weyl and dirac semimetals. *Nature Communications*, 5:5161, 2014.
- [10] L. X. Yang, Z. K. Liu, Y. Sun, H. Peng, H. F. Yang, T. Zhang, B. Zhou, Y. Zhang, Y. F. Guo, M. Rahn, D. Prabhakaran, Z. Hussain, S. K. Mo, C. Felser, B. Yan, and Y. L. Chen. Weyl semimetal phase in the non-centrosymmetric compound taas. *Nat. Phys.*, 11(9):728–732, 2015.
- [11] Su-Yang Xu, Nasser Alidoust, Ilya Belopolski, Zhujun Yuan, Guang Bian, Tay-Rong Chang, Hao Zheng, Vladimir N. Strocov, Daniel S. Sanchez, Guoqing Chang, Chenglong Zhang,

- Daixiang Mou, Yun Wu, Lunan Huang, Chi-Cheng Lee, Shin-Ming Huang, BaoKai Wang, Arun Bansil, Horng-Tay Jeng, Titus Neupert, Adam Kaminski, Hsin Lin, Shuang Jia, and M. Zahid Hasan. Discovery of a weyl fermion state with fermi arcs in niobium arsenide. *Nat. Phys.*, 11(9):748–754, 2015.
- [12] Z. K. Liu, L. X. Yang, Y. Sun, T. Zhang, H. Peng, H. F. Yang, C. Chen, Y. Zhang, Y. F. Guo, D. Prabhakaran, M. Schmidt, Z. Hussain, S. K. Mo, C. Felser, B. Yan, and Y. L. Chen. Evolution of the fermi surface of weyl semimetals in the transition metal pnictide family. *Nat. Mater.*, 15:27–31, 2016.
- [13] B. Q. Lv, N. Xu, H. M. Weng, J. Z. Ma, P. Richard, X. C. Huang, L. X. Zhao, G. F. Chen, C. E. Matt, F. Bisti, V. N. Strocov, J. Mesot, Z. Fang, X. Dai, T. Qian, M. Shi, and H. Ding. Observation of weyl nodes in taas. *Nat. Phys.*, 11(9):724–727, 2015.
- [14] B. Q. Lv, S. Muff, T. Qian, Z. D. Song, S. M. Nie, N. Xu, P. Richard, C. E. Matt, N. C. Plumb, L. X. Zhao, G. F. Chen, Z. Fang, X. Dai, J. H. Dil, J. Mesot, M. Shi, H. M. Weng, and H. Ding. Observation of fermi-arc spin texture in taas. *Phys. Rev. Lett.*, 115:217601, 2015.
- [15] Alexey A. Soluyanov, Dominik Gresch, Zhijun Wang, QuanSheng Wu, Matthias Troyer, Xi Dai, and B. Andrei Bernevig. Type-ii weyl semimetals. *Nature*, 527(7579):495–498, 2015.
- [16] Yan Sun, Shu-Chun Wu, Mazhar N. Ali, Claudia Felser, and Binghai Yan. Prediction of weyl semimetal in orthorhombic mote₂. *Phys. Rev. B*, 92:161107, 2015.
- [17] Zhijun Wang, Dominik Gresch, Alexey A. Soluyanov, Weiwei Xie, S. Kushwaha, Xi Dai, Matthias Troyer, Robert J. Cava, and B. Andrei Bernevig. mote₂. *Phys. Rev. Lett.*, 117:056805, 2016.
- [18] Tay-Rong Chang, Su-Yang Xu, Guoqing Chang, Chi-Cheng Lee, Shin-Ming Huang, BaoKai Wang, Guang Bian, Hao Zheng, Daniel S. Sanchez, Ilya Belopolski, Nasser Alidoust, Madhab Neupane, Arun Bansil, Horng-Tay Jeng, Hsin Lin, and M. Zahid Hasan. Prediction of an arc-tunable weyl fermion metallic state in moxw₁xte₂. *Nature Communications*, 7:10639, 2016.
- [19] R Clarke, E Marseglia, and H P Hughes. A low-temperature structural phase transition in β -MoTe₂. *Philosophical Magazine Part B*, 38:121–126, 1978.
- [20] Lunan Huang, Timothy M. McCormick, Masayuki Ochi, Zhiying Zhao, Michi-To Suzuki, Ryotaro Arita, Yun Wu, Daixiang Mou, Huibo Cao, Jiaqiang Yan, Nandini Trivedi, and Adam Kaminski. Spectroscopic evidence for a type ii weyl semimetallic state in mote₂. *Nat.*

- Mater.*, 15(11):1155–1160, 2016.
- [21] A. Tamai, Q. S. Wu, I. Cucchi, F. Y. Bruno, S. Riccò, T. K. Kim, M. Hoesch, C. Barreateau, E. Giannini, C. Besnard, A. A. Soluyanov, and F. Baumberger. Fermi arcs and their topological character in the candidate type-ii weyl semimetal mote_2 . *Phys. Rev. X*, 6:031021, 2016.
 - [22] Ke Deng, Guoliang Wan, Peng Deng, Kenan Zhang, Shijie Ding, Eryin Wang, Mingzhe Yan, Huaqing Huang, Hongyun Zhang, Zhilin Xu, Jonathan Denlinger, Alexei Fedorov, Haitao Yang, Wenhui Duan, Hong Yao, Yang Wu, Shoushan Fan, Haijun Zhang, Xi Chen, and Shuyun Zhou. Experimental observation of topological fermi arcs in type-ii weyl semimetal mote_2 . *Nat. Phys.*, 12(12):1105–1110, 2016.
 - [23] F. Y. Bruno, A. Tamai, Q. S. Wu, I. Cucchi, C. Barreateau, A. de la Torre, S. McKeown Walker, S. Riccò, Z. Wang, T. K. Kim, M. Hoesch, M. Shi, N. C. Plumb, E. Giannini, A. A. Soluyanov, and F. Baumberger. Observation of large topologically trivial fermi arcs in the candidate type-ii weyl semimetal WTe_2 . *Phys. Rev. B*, 94:121112, 2016.
 - [24] Yun Wu, Daixiang Mou, Na Hyun Jo, Kewei Sun, Lunan Huang, S. L. Bud’ko, P. C. Canfield, and Adam Kaminski. Observation of fermi arcs in the type-ii weyl semimetal candidate wte_2 . *Phys. Rev. B*, 94:121113, 2016.
 - [25] J. Sánchez-Barriga, M. G. Vergniory, D. Evtushinsky, I. Aguilera, A. Varykhalov, S. Blügel, and O. Rader. Surface fermi arc connectivity in the type-ii weyl semimetal candidate wte_2 . *Phys. Rev. B*, 94:161401, 2016.
 - [26] Chenlu Wang, Yan Zhang, Jianwei Huang, Simin Nie, Guodong Liu, Aiji Liang, Yuxiao Zhang, Bing Shen, Jing Liu, Cheng Hu, Ying Ding, Defa Liu, Yong Hu, Shaolong He, Lin Zhao, Li Yu, Jin Hu, Jiang Wei, Zhiqiang Mao, Youguo Shi, Xiaowen Jia, Fengfeng Zhang, Shenjin Zhang, Feng Yang, Zhimin Wang, Qinqun Peng, Hongming Weng, Xi Dai, Zhong Fang, Zuyan Xu, Chuangtian Chen, and X. J. Zhou. Observation of fermi arc and its connection with bulk states in the candidate type-ii weyl semimetal wte_2 . *Phys. Rev. B*, 94:241119, 2016.
 - [27] Ilya Belopolski, Daniel S. Sanchez, Yukiaki Ishida, Xingchen Pan, Peng Yu, Su-Yang Xu, Guoqing Chang, Tay-Rong Chang, Hao Zheng, Nasser Alidoust, Guang Bian, Madhab Neupane, Shin-Ming Huang, Chi-Cheng Lee, You Song, Haijun Bu, Guanghou Wang, Shisheng Li, Goki Eda, Horng-Tay Jeng, Takeshi Kondo, Hsin Lin, Zheng Liu, Fengqi Song, Shik Shin, and M. Zahid Hasan. Discovery of a new type of topological weyl fermion semimetal state in

- moxw1?xte2. *Nature Communications*, 7:13643, 2016.
- [28] Note that the possible phase transition between 4 or 8 wps (as indicated in fig.1, bottom right) will not play a role here since still there will be a very large topological fermi arc.
- [29] Hao Zheng, Guang Bian, Guoqing Chang, Hong Lu, Su-Yang Xu, Guangqiang Wang, Tay-Rong Chang, Songtian Zhang, Ilya Belopolski, Nasser Alidoust, Daniel S. Sanchez, Fengqi Song, Horng-Tay Jeng, Nan Yao, Arun Bansil, Shuang Jia, Hsin Lin, and M. Zahid Hasan. Atomic-scale visualization of quasiparticle interference on a type-ii weyl semimetal surface. *Phys. Rev. Lett.*, 117:266804, 2016.
- [30] Zhoushen Huang, Tanmoy Das, Alexander V. Balatsky, and Daniel P. Arovas. Stability of weyl metals under impurity scattering. *Phys. Rev. B*, 87:155123, 2013.
- [31] T.O. Wehling, A.M. Black-Schaffer, and A.V. Balatsky. Dirac materials. *Advances in Physics*, 63(1):1–76, 2014.
- [32] Swantje Heers. *Effect of spin-orbit scattering on transport properties of low-dimensional dilute alloys*. PhD thesis, RWTH Aachen University, 2011.
- [33] Bernd Zimmermann, Phivos Mavropoulos, Nguyen H. Long, Christian-Roman Gerhorst, Stefan Blügel, and Yuriy Mokrousov. Fermi surfaces, spin-mixing parameter, and colossal anisotropy of spin relaxation in transition metals from ab initio theory. *Physical Review B*, 93(14):144403, apr 2016.
- [34] Nguyen H. Long, Phivos Mavropoulos, Bernd Zimmermann, David S. G. Bauer, Stefan Blügel, and Yuriy Mokrousov. Spin relaxation and spin Hall transport in 5 d transition-metal ultrathin films. *Physical Review B*, 90:064406, 2014.
- [35] Rudolf Zeller. An elementary derivation of lloyd’s formula valid for full-potential multiple-scattering theory. *Journal of Physics: Condensed Matter*, 16(36):6453, 2004.
- [36] Baojie Feng, Yang-Hao Chan, Ya Feng, Ro-Ya Liu, Mei-Yin Chou, Kenta Kuroda, Koichiro Yaji, Ayumi Harasawa, Paolo Moras, Alexei Barinov, Walid Malaeb, Cédric Bareille, Takeshi Kondo, Shik Shin, Fumio Komori, Tai-Chang Chiang, Youguo Shi, and Iwao Matsuda. Spin texture in type-ii weyl semimetal wte₂. *Phys. Rev. B*, 94:195134, 2016.
- [37] We would like to mention that the tiny differences between the two inequivalent top and bottom surfaces which originate from the inversion asymmetric crystal structure characterizing both wte₂ and mote₂ (see supplementary material for theoretical results) can also not be resolved experimentally.

- [38] Pedram Roushan, Jungpil Seo, Colin V. Parker, Y. S. Hor, D. Hsieh, Dong Qian, Anthony Richardella, M. Z. Hasan, R. J. Cava, and Ali Yazdani. Topological surface states protected from backscattering by chiral spin texture. *Nature*, 460(7259):1106–1109, 2009.
- [39] Tong Zhang, Peng Cheng, Xi Chen, Jin-Feng Jia, Xucun Ma, Ke He, Lili Wang, Haijun Zhang, Xi Dai, Zhong Fang, Xincheng Xie, and Qi-Kun Xue. Experimental demonstration of topological surface states protected by time-reversal symmetry. *Phys. Rev. Lett.*, 103:266803, 2009.
- [40] Paolo Sessi, Felix Reis, Thomas Bathon, Konstantin A. Kokh, Oleg E. Tereshchenko, and Matthias Bode. Signatures of dirac fermion-mediated magnetic order. *Nature Communications*, 5:5349, 2014.
- [41] Ilija Zeljkovic, Yoshinori Okada, Cheng-Yi Huang, R. Sankar, Daniel Walkup, Wenwen Zhou, Maksym Serbyn, Fangcheng Chou, Wei-Feng Tsai, Hsin Lin, A. Bansil, Liang Fu, M. Zahid Hasan, and Vidya Madhavan. Mapping the unconventional orbital texture in topological crystalline insulators. *Nat. Phys.*, 10(8):572–577, 2014.
- [42] Sangjun Jeon, Brian B. Zhou, Andras Gyenis, Benjamin E. Feldman, Itamar Kimchi, Andrew C. Potter, Quinn D. Gibson, Robert J. Cava, Ashvin Vishwanath, and Ali Yazdani. Landau quantization and quasiparticle interference in the three-dimensional dirac semimetal Cd_3As_2 . *Nat. Mater.*, 13(9):851–856, 2014.
- [43] Paolo Sessi, Yan Sun, Thomas Bathon, Florian Glott, Zhilin Li, Hongxiang Chen, Liwei Guo, Xiaolong Chen, Marcus Schmidt, Claudia Felser, Binghai Yan, and Matthias Bode. Impurity screening and stability of fermi arcs against coulomb and magnetic scattering in a weyl mononpnictide. *Phys. Rev. B*, 95:035114, 2017.
- [44] P. Sessi, P. Rüßmann, T. Bathon, A. Barla, K. A. Kokh, O. E. Tereshchenko, K. Fauth, S. K. Mahatha, M. A. Valbuena, S. Godey, F. Glott, A. Mugarza, P. Gargiani, M. Valvidares, N. H. Long, C. Carbone, P. Mavropoulos, S. Blügel, and M. Bode. Superparamagnetism-induced mesoscopic electron focusing in topological insulators. *Phys. Rev. B*, 94:075137, 2016.
- [45] J. I. Pascual, G. Bihlmayer, Yu. M. Koroteev, H.-P. Rust, G. Ceballos, M. Hansmann, K. Horn, E. V. Chulkov, S. Blügel, P. M. Echenique, and Ph. Hofmann. Role of spin in quasiparticle interference. *Phys. Rev. Lett.*, 93:196802, 2004.
- [46] Paolo Sessi, Rudro R. Biswas, Thomas Bathon, Oliver Storz, Stefan Wilfert, Alessandro Barla, Konstantin A. Kokh, Oleg E. Tereshchenko, Kai Fauth, Matthias Bode, and Alexander V.

- Balatsky. Dual nature of magnetic dopants and competing trends in topological insulators. *Nature Communications*, 7:12027 EP –, 2016.
- [47] Zhong et al. Lin. Defect engineering of two-dimensional transition metal dichalcogenides. *2D Mater*, 3:022002, 2016.
- [48] Jinhua Hong, Zhixin Hu, Matt Probert, Kun Li, Danhui Lv, Xinan Yang, Lin Gu, Nannan Mao, Qingliang Feng, Liming Xie, Jin Zhang, Dianzhong Wu, Zhiyong Zhang, Chuanhong Jin, Wei Ji, Xixiang Zhang, Jun Yuan, and Ze Zhang. Exploring atomic defects in molybdenum disulphide monolayers. *Nature Communications*, 6:6293, 2015.
- [49] Hye Yun Jeong, Si Young Lee, Thuc Hue Ly, Gang Hee Han, Hyun Kim, Honggi Nam, Zhao Jiong, Bong Gyu Shin, Seok Joon Yun, Jaesu Kim, Un Jeong Kim, Sungwoo Hwang, and Young Hee Lee. Visualizing point defects in transition-metal dichalcogenides using optical microscopy. *ACS Nano*, 10:770–777, 2016.
- [50] Su-Yang Xu, Madhab Neupane, Ilya Belopolski, Chang Liu, Nasser Alidoust, Guang Bian, Shuang Jia, Gabriel Landolt, Batosz Slomski, J. Hugo Dil, Pavel P. Shibayev, Susmita Basak, Tay-Rong Chang, Horng-Tay Jeng, Robert J. Cava, Hsin Lin, Arun Bansil, and M. Zahid Hasan. Unconventional transformation of spin dirac phase across a topological quantum phase transition. *Nature Communications*, 6:6870, 2015.
- [51] A. Narayanan, M. D. Watson, S. F. Blake, N. Bruyant, L. Drigo, Y. L. Chen, D. Prabhakaran, B. Yan, C. Felser, T. Kong, P. C. Canfield, and A. I. Coldea. Linear magnetoresistance caused by mobility fluctuations in n -doped cd_3as_2 . *Phys. Rev. Lett.*, 114:117201, Mar 2015.
- [52] Yupeng Li, Zhen Wang, Pengshan Li, Xiaojun Yang, Zhixuan Shen, Feng Sheng, Xiaodong Li, Yunhao Lu, Yi Zheng, and Zhu-An Xu. Negative magnetoresistance in weyl semimetals nbas and nbp: Intrinsic chiral anomaly and extrinsic effects. *Frontiers of Physics*, 12(3):127205, 2017.
- [53] Mazhar N. Ali, Jun Xiong, Steven Flynn, Jing Tao, Quinn D. Gibson, Leslie M. Schoop, Tian Liang, Neel Haldolaarachchige, Max Hirschberger, N. P. Ong, and R. J. Cava. Large, non-saturating magnetoresistance in wte2. *Nature*, 514(7521):205–208, 10 2014.
- [54] Yaojia Wang, Erfu Liu, Huimei Liu, Yiming Pan, Longqiang Zhang, Junwen Zeng, Yajun Fu, Miao Wang, Kang Xu, Zhong Huang, Zhenlin Wang, Hai-Zhou Lu, Dingyu Xing, Baigeng Wang, Xiangang Wan, and Feng Miao. Gate-tunable negative longitudinal magnetoresistance in the predicted type-ii weyl semimetal wte2. *Nature Communications*, 7:13142 EP –, 10 2016.